The Potentialities of Raman and XPS Techniques to Evaluate the Corrosion Products Formed on the 2198-T851 Aluminium Alloy Exposed to Sodium Chloride Solution

M. O. A. Ferreira[a] , **J. P. L. Nascimento**[a] , **N. B. Leite**[a] , **A. de Siervo**[b] , **G. L. Fernandes**[c] ,

A. R. Vaz[d] , **R. V. Gelamo**[e] , **I. V. Aoki**[f] , **J. A. Moreto**[a]*

[a]*Universidade Federal do Triângulo Mineiro (UFTM), Instituto de Ciências Exatas, Naturais e Educação, Avenida Doutor Randolfo Borges Júnior, Univerdecidade, Uberaba, MG, Brasil.*
[b]*Universidade Estadual de Campinas (UNICAMP), Departamento de Física, Grupo de Ciências de Superfície, Campinas, SP, Brasil.*
[c]*Universidade Federal de Uberlândia (UFU), Avenida João Naves de Ávila, Uberlândia, MG, Brasil.*
[d]*Universidade Estadual de Campinas (UNICAMP), Centro de Componentes Semicondutores e Nanotecnologias (CCSNano), Campinas, SP, Brasil.*
[e]*Universidade Federal do Triângulo Mineiro (UFTM), Instituto de Ciências Tecnológicas e Exatas, Avenida Doutor Randolfo Borges Júnior, Univerdecidade, Uberaba, MG, Brasil.*
[f]*Universidade de São Paulo (USP), Escola Politécnica, Departamento de Engenharia Química, Av. Prof. Luciano Gualberto, Cidade Universitária, São Paulo, SP, Brasil.*

The aerospace industry is constantly looking for innovative materials that exhibit good mechanical and corrosion properties. The 2198-T851 (Al-Cu-Li) alloy was developed to replace the conventional Al-Cu-Mg in aircraft structures. Despite the usefulness of the 2198-T851 alloy, its performance may be affected when subjected to an aggressive medium containing chloride ions. The deposition of Nb_2O_5 coatings by using the reactive sputtering technique on the 2198-T851 alloy surface appears as a powerful tool to improve the corrosion resistance of this material. Recently, groundbreaking research findings have demonstrated the positive effect of Nb_2O_5 coatings on corrosion protection of alloy 2198-T851. However, the corrosion products originated from the 2198-T851 aluminium alloy are poorly understood. The use of Raman spectroscopy and XPS techniques may help to shed some light on the corrosion products of 2198-T851 alloy. Results demonstrated the corrosion products are mainly composed by $CuCl_2$ x H_2O, $CuCl$, $Cu_2Cl(OH)_3$, $Al(OH)_3$, and $AlO(OH)$.

Keywords: *Al-Cu-Li alloy, Raman, XPS technique, Corrosion products, Aircraft industry.*

1. Introduction

The aircraft industry is always demanding for innovative materials with higher mechanical performances as well as good corrosion properties[1]. The 3rd generation of Al-Cu-Li alloys appear as feasible replacements of traditional 2xxx series alloys and constitute a promising group of metallic materials having noteworthy prospective applications in this field[1,2]. The 2198-T851 (Al-Cu-Li) aluminium alloy is based on weight reduction, since it presents lower density, higher strength, and toughness than other aluminium alloys from this series[3]. However, as mentioned by Georgoulis and colleagues[4], Al-Cu-Li alloys were found to be highly susceptible to localised corrosion. In fact, different behaviour in the corrosion attack mechanisms between Al-Cu-Li and conventional Al-Cu-Mg alloys were reported by Moreto et al.[5].

As mentioned by Donatus et al.[6] and Araujo et al.[7,8], the predominant mode of corrosion on 2198-T851 aluminium alloy is intragranular, propagating through bands parallel to the {111} aluminium planes. In addition to these observations, Moreto et al.[5] emphasize that aluminium alloys are more likely to undergo localised corrosion, as a result of defects on the passive protective film occurring near secondary phase particle. In fact, 2198-T851 aluminium alloy exhibits a complex microstructure due to the presence of Al_3Li, $T_1(Al_2CuLi)$, $\theta'(Al_2Cu)$ and S (Al_2CuMg) precipitates. These precipitates are directly linked to the alloy composition and the thermomechanical processing[9]. Nonetheless, these phases can promote galvanic coupling with the aluminium matrix by making it very sensitive to localised corrosion processes. When 2198-T851 aluminium alloy is exposed to an aggressive anions like Cl⁻, the pitting corrosion process is enhanced, i.e., aggressive anions can be transported through a passive film on aluminium and reach the aluminium/oxide interface[10].

Surface treatments have been widely used to improve the base material corrosive properties. Since they give rise to a physical protective barrier that interfaces with the,

possibly hostile, environment. Plasma surface treatment appears as a powerful tool in surface modification of metallic materials because of its superior efficiency, green chemical method as well as low cost[11]. Recently, groundbreaking research findings have demonstrated the positive effect of Nb_2O_5 coatings on the corrosion protection of 2xxx series aluminium alloys.

The first work that should be mentioned was carried out by Moreto et al.[12] and focused on the surface modification of 2524-T3 (Al-Cu-Mg) aluminium alloy substrates by using Nb_2O_5 coatings employing reactive sputtering technique. The Nb_2O_5 coating was able to delay the onset of corrosion process as demonstrated by SVET, pH micro-potentiometry and EIS techniques. In addition to the good corrosive properties, the Nb_2O_5 coating also improved the wear performance of 2524-T3 aluminium alloy. The corrosion behaviour of reactive sputtering deposition Nb_2O_5 based coating on the 2198-T851 aluminium alloy was verified by Freitas et al.[13], which demonstrated the reactive plasma technique created a barrier layer, promoting a difference about 210 mV between the corrosion potential (E_{corr}) and pitting potential ($E_{pitting}$). The improvement of the corrosion properties was also verified by using electrochemical impedance spectroscopy, which demonstrated an increasing of impedance modulus more than one order. Furthermore, the coated material presented phase angle values closer to -90°, indicating a capacitive effect of the Nb_2O_5 coating. The effect of Nb_2O_5 thin film on the long-term immersion corrosion of the 2198-T851 aluminium alloy was proposed by Ferreira et al.[14]. Results demonstrated the 2198-T851 aluminium alloy coated with Nb_2O_5 thin film immersed in sodium chloride solution (0.6 mol L^{-1}) during 720 h exhibits the same behaviour as the base material for 3 h of immersion as showed by the EIS tests. These findings are in line with the work presented by Freitas et al.[13], demonstrating the deposited thin film by using reactive sputtering technique was able to increase the corrosion resistance of the 2198-T851 aluminium alloy.

A significant amount of work has already been conducted on electrochemical and corrosion-fatigue behaviour of the 2198-T851 aluminium alloy. However, most of them do not explain in detail the corrosion products that are formed when 2198-T851 aluminium alloy is exposed to an aggressive medium containing chloride ions as well as their influence on the fatigue behaviour, mainly in the crack closure phenomenon. Corrosion and fatigue of aluminium alloys are major issues for the in-service life assessment of aircraft structures and for the management of aging air fleets. The understanding of the corrosion-fatigue phenomena, kinetics, and micromechanisms acting is essential for life prediction, as well as for the development of alloys with increased fatigue performance. For this reason, the development of corrosion studies that will allow a greater understanding of corrosion-fatigue processes is very important. Based on these findings, this research presents new discoveries regarding the corrosion products formed on the 2198-T851 and 2198-T851/Nb_2O_5 specimens. The use of Raman spectroscopy combined to X-ray photoelectron spectroscopy (XPS) techniques may help to shed some light on the corrosion products formed on the coated and uncoated 2198-T851 aluminium alloy when exposed to sodium chloride solution.

2. Experimental

2.1. Material and methods

In the present work, the 2198-T851 (Solution Heat Treated, Cold Worked, and Artificially Aged) aluminium alloy was used as received condition. Prior to the functionalization of the specimens using reactive sputtering technique, all samples were cut into standardized sizes (1 cm x 1 cm) and mechanically polished by using silicon carbide (SiC) sandpaper at 800, 1200, 2400 and 4000#. The polishing process was finished using 3, 2 and 1μm diamond pastes. After, the specimens were washed in distilled water and then degreased in isopropyl alcohol for a period of 10 min and conditioned in a desiccator. The Nb_2O_5 thin films were deposited on the short transverse direction in all specimens of 2198-T851 aluminium alloy by using the reactive sputtering technique at the Laboratory of Thin Films and Plasma Processes of the Federal University of Triângulo Mineiro, UFTM, Brazil. The other regions of the samples were delimited with bee wax for corrosion studies. The deposition process has optimized parameters and further details can be found in references[12-14].

Samples of 2198-T851 aluminium alloy with and without Nb_2O_5 thin films were monitored in 0.6 mol L^{-1} NaCl solution during 24 h of immersion. After the immersion tests were performed, the morphology of the coated and uncoated 2198-T851 aluminium alloy was accessed by using optical microscopy (Nova 156-T microscope) and scanning electron microscopy (FEG- SEM JEOL 7001 F equipped with an Oxford light elements EDX detector). This procedure was used to assess the morphological changes and to detect modifications on the surface composition.

The focused ion beam (FIB) technique was used in the present study to determine the depth of the pits formed on the coated and uncoated 2198-T851 aluminium alloy surfaces. The FIB system model used in our experiment is a dual beam from FEI (Dual Beam Nova Nanolab - Model Nova 200). This system combines an ion beam column with a scanning electron microscope (SEM) working at coincidence on the sample. This allows us to monitor ion beam processing with simultaneous SEM imaging. The FIB column is equipped with a Ga^+ source and has a minimum spot size of 5 nm at 30 kV whereas the SEM column has a thermal field emission gun which can achieve a 5 nm resolution over a wide energy range. The FIB technique for cross-section is well-known and very useful. Specifically, in the present work, the FIB technique was used to measure the depth of pits formed on the coated and uncoated 2198-T851 aluminium alloy. Initially, a layer of sacrificial platinum is deposited to protect the surface and facilitate visualization and measurements of the subsequent layers. Then, it was used an ion beam (30 kV, 3 nA) to pulverize the surface and then polish with the ion beam (30 kV, 1 nA) to optimize the contrast between the layers for thickness measurements.

Corrosion products formed on the surface of coated and uncoated 2198-T851 aluminium alloy during the immersion tests were evaluated by using Raman spectroscopy and XPS techniques. For this purpose, a LabRam HR Evolution Raman spectrometer was used. An Olympus XB41 optical microscope with software controlled XY table orientation was connected to the spectrometer.

The Potentialities of Raman and XPS Techniques to Evaluate the Corrosion Products Formed on the 2198-T851 Aluminium Alloy Exposed to Sodium Chloride Solution

3

The samples were excited with an Ar^+ laser (532 nm) with a power of 12 mW (25% of the maximum available) and a 600-line/mm grating with a confocal hole of 250 μm. Raman spectra were acquired using the scan mode method at room temperature, taking 20 s per window and 9 accumulations (the window travels 1/9 of its dimensions per accumulation until it covers the entire needed range of the spectrum). The analyses were performed by using LabSpec software (LabSpec 6 Spectroscopy Suite) from HORIBA Scientific. In addition, the analyses were made easier using HORIBA Scientific's LabSpec software (LabSpec 6 Spectroscopy Suite), which allowed better visualization of the results in Raman Microscopy Mappings. For the uncoated specimens, it was used a higher power (100% - 50 mW). XPS measurements were performed using a SPECS Phoibos high resolution hemispherical analyser with multiple channeltron detection and Al Kα x-ray source. These spectra were fitted with the Doniach and Sunjic[15] line shape characterized by a Lorentzian width Γ, which considers the finite core-hole lifetime, and by the asymmetry parameter α that describes low-energy electron hole pair excitations near the Fermi level. All peaks were convoluted to a Gaussian distribution (fixed width of 1.0 eV) that describes the instrumental broadening, phonon contributions, and sample in homogeneities. The inelastic background contribution was removed using the Shirley type background.

3. Results and Discussions

Figure 1 displays the optical micrographs images for the 2198-T851 aluminium alloy exposed for a period of 3, 15 and 24 h of immersion in 0.6 mol L^{-1} NaCl solution. As can be seen, 2198-T851 aluminium alloy exhibits intense activity during the first 24 h of immersion, as well as pitting in the rolling direction. These findings clearly indicate that the spontaneously formed thin film of Al_2O_3 on the AA2198-T851 surface is not able to protect it from the advance of the corrosion process. As mentioned by Metikoš-Huković et al.[16], corrosion pits are initiated at the oxide layer in sites weakened by chloride attack, normally chemical or physical heterogeneities at the surface, such as inclusions, second-phase particles, flaws, mechanical damage, or dislocations. According to the literature[17], pitting corrosion follows three possible mechanisms: penetration, adsorption, and film-breaking. The contributions of submicrometric intermetallic particles present in the 2198-T851 aluminium alloy should be highlighted, since these phases promote galvanic coupling, leading to the preferential dissolution of the nearby matrix, with formation of preferential sites for pitting initiation. In 3 h of immersion, a severe localised corrosion (SLC) process can already be verified, which is typical for the studied material and is related to the presence of T_1 phase[7]. Subsequently, a proposed corrosion mechanism will be presented for the 2198-T851 aluminium alloy exposed to a solution containing chloride ions.

Figure 2 shows a schematic assembly of the 2198-T851 aluminium alloy containing Nb_2O_5 thin film after 3, 15 and 24 h of immersion in 0.6 mol L^{-1} NaCl solution. Impressively, Nb_2O_5 coating deposited on the 2198-T851 alloy surface by reactive sputtering technique acts as a protective barrier against localised corrosion process. Even after 24 h of immersion in 0.6 mol L^{-1} NaCl, the Nb_2O_5 thin film maintains its integrity practically intact.

The proposed corrosion mechanism for the 2198-T851 aluminium alloy exposed to sodium chloride solution is quite complex and can be seen in Figure 3.
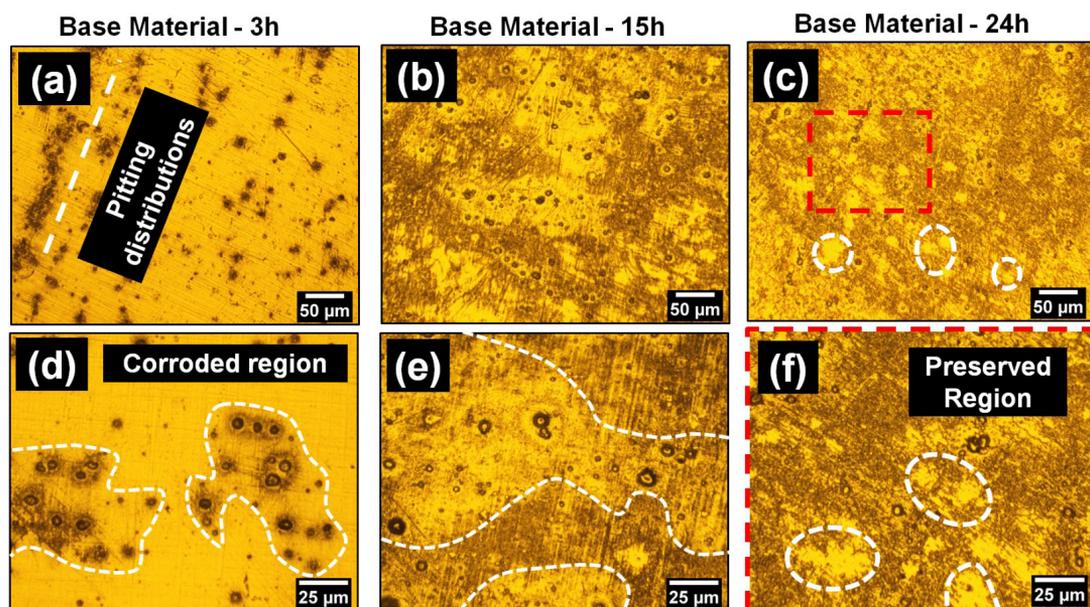
Figure 1. (a) optical images after the corrosion immersion tests for the base material, **(a, d)** 3 h, **(b, e)** 15 h, and **(c, f)** 24 h of immersion in 0.6 mol L^{-1} NaCl solution.
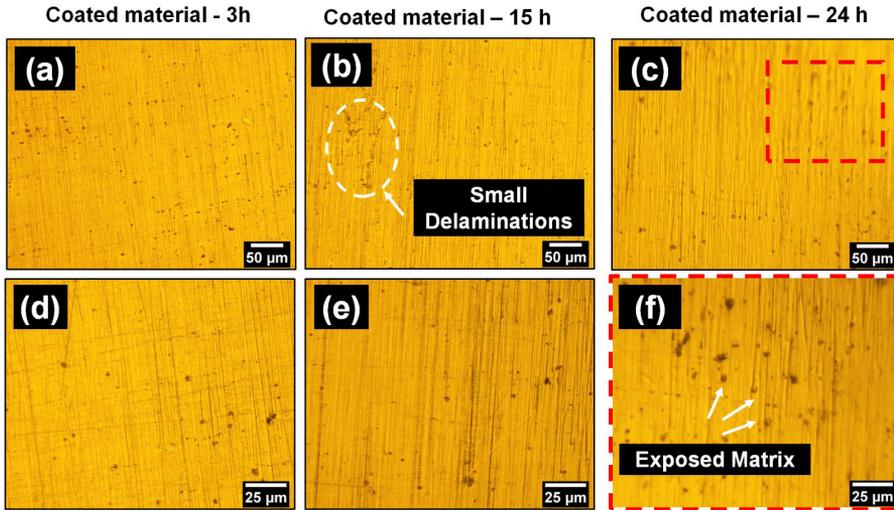
Figure 2. Optical images after the corrosion immersion tests for the 2198-T851 aluminium alloy containing Nb_2O_5 thin film, **(a, d)** 3 h, **(b, e)** 15 h, and **(c, f)** 24 h of immersion in 0.6 mol L^{-1} NaCl solution.
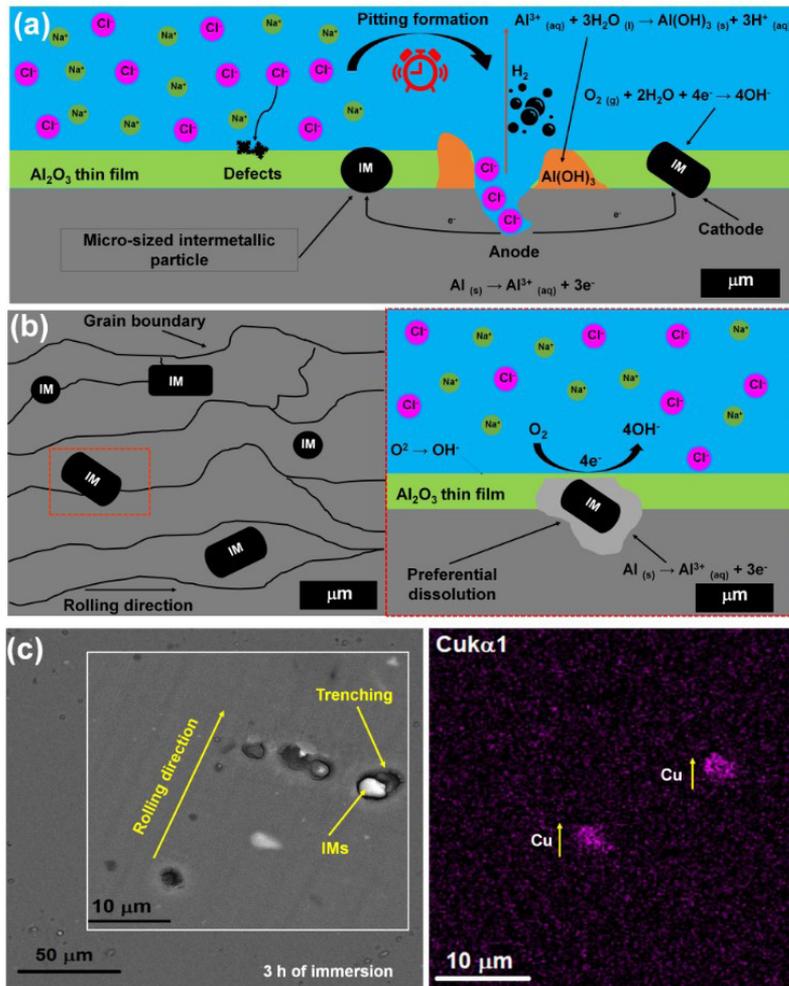
Figure 3. (a) Schematic drawing of the mechanism of pitting corrosion in 2198-T851 aluminium alloy exposed to an aggressive medium, **(b)** schematic illustration related to the galvanic coupling between the submicrometric intermetallic particles and 2198-T851 aluminium matrix, and **(c)** SEM image of the 2198-T851 aluminium alloy surface after 3 h of immersion tests in 0.6 mol L^{-1} NaCl solution as well as the representative EDX map.

The Potentialities of Raman and XPS Techniques to Evaluate the Corrosion Products Formed on the 2198-T851
Aluminium Alloy Exposed to Sodium Chloride Solution

5

At first, it can be considered that pits are initiate due to local rupture of the Al_2O_3 thin film or the presence of defects, propagating in a self-sustaining manner[18] (see Figure 3a). A representative assembly of the corrosion mechanism due to the submicrometric intermetallic particles present on the 2198-T851 aluminium matrix as well as the existence of galvanic coupling is shown in Figure 3b. The pitting corrosion initiates at the interface of cathodic intermetallic particle, acting as a site for the cathodic reaction (oxygen reduction reaction). Moreto et al.[4] demonstrated by using scanning vibrating electrode technique (SVET) and electrochemical impedance spectroscopy (EIS) tests the localised feature of the 2198-T851 aluminium alloy is directly linked to the existence of intermetallic particles that can present cathodic or anodic behaviour in relation to the aluminium matrix. This phenomenon introduces an alkaline environment around the intermetallic particle, promoting a localised dissolution of the protective thin film of alumina. Figure 3cexhibits the SEM image of the uncoated 2198-T851 aluminium alloy exposed to 0.6 mol L^{-1} NaCl solution during 3 h of immersion. According to Witharamage et al.[19], the interaction between the metallic matrix and the sodium chloride electrolyte causes rapid oxidation of the 2198-T851 aluminium alloy, leading to the pit initiation. The cathodic nature of these intermetallic particles can be confirmed with the SEM image, which showed the dissolution of the 2198-T851 aluminium alloy around the mentioned particles. In addition, the formation of pits in the rolling direction of the 2198-T851 aluminium alloy can be verified, which combines in a severe localised corrosion process. The corroded areas coincide with the presence of Cu element as displayed in EDX map.

Figure 4 shows the formation of a dense film on the 2198-T851 aluminium alloy surface, probably Al_2O_3, after 24 h of immersion in 0.6 mol L^{-1} NaCl solution. Further information regarding the nature of the coating will be made with the aid of the XPS and Raman spectroscopy techniques and discussed below. The results also demonstrated dissolution of aluminium matrix, formation of trenching in the vicinity

of an intermetallic particle that has been removed from the surface as well as the presence of corrosion products. Another corrosion mechanism may be related to the existence of T_1 nanometric particles as displayed in Figure 5a. As mentioned by Moreto et al.[20] and confirmed by Araújo et al.[21], when 2198-T851 aluminium alloy is exposed to a corrosive environment, T_1 precipitates are anodic with respect to the aluminium matrix, promoting their dissolution. As the corrosion process progresses, T_1 becomes cathodic due to the selective dissolution of aluminium and lithium elements, increasing the Cu amount on the 2198-T851 aluminium alloy matrix as represented by Figure 5b.
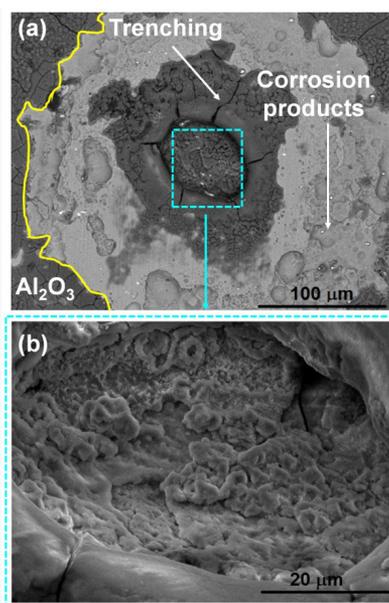
Figure 4. (a) SEM image of the 2198-T851 aluminium alloy surface after 24 h of immersion tests in 0.6 mol L^{-1} NaCl solution and **(b)** magnified region of the sample.
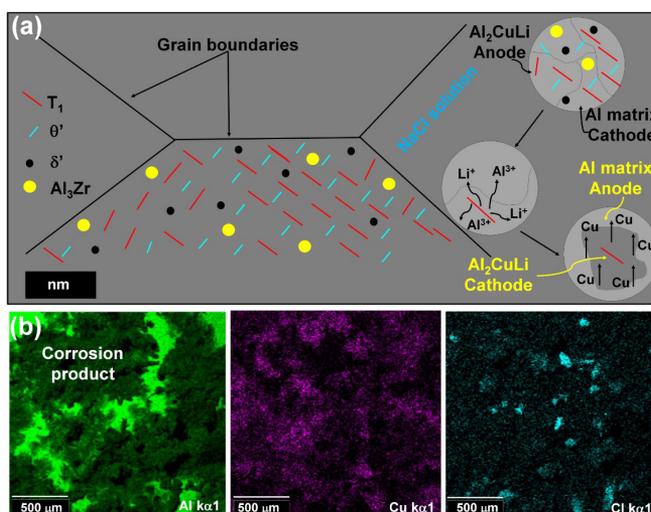
Figure 5. (a) Schematic illustration of the localised corrosion mechanism associated to the presence of T_1 nanometric particles as proposed by Moreto et al.[20] and proved by Araújo et al.[21], and **(b)** EDX maps, confirming the presence of Cu element on the 2198-T851 aluminium alloy matrix.

Figure 6a shows a schematic drawing to elucidate the corrosion mechanism of coated 2198-T851 aluminium alloy exposed to 0.6 mol L^{-1} NaCl solution. Although the Nb_2O_5 thin film has acted as a protective barrier against localised corrosion process, it was possible to verify a small uncovered region on the surface of the analysed sample after 24 h of immersion. In summary, when 2198-T851 aluminium alloy containing Nb_2O_5 thin film is exposed to 0.6 mol L^{-1} NaCl solution, the Cl^- ions permeate through the coating defects, promoting the aluminium matrix dissolution. The defects presented in the Nb_2O_5 thin films were originated from the absence of heat treatment during and after the reactive sputtering deposition. Many studies have evidenced the effect of the grain and crystallite sizes on the corrosion of a wide range of materials[22,23].

The advancement of the corrosion process causes the Cl^- ions to reach the aluminium alloy substrate, initiating the formation of a pitting as discussed in Figure 3. In this sense, the propagation of corrosion process under the thin film, leading to coating detachment. These observations are supported by the schematic drawing, which shows the absence of Nb_2O_5 in the delimited zones (see Figure 6bc).

As already mentioned before, the FIB technique was applied in the present work to determine the cross-sectional of the selected pit formed on the coated and uncoated 2198-T851 aluminium alloy surfaces after 24 h of immersion in 0.6 mol L^{-1} NaCl. Figure 7a displays an overview of the 2198-T851 aluminium alloy matrix as well as the pit distribution. Figure 7b shows the magnification of the selected pit for the cross section performing.
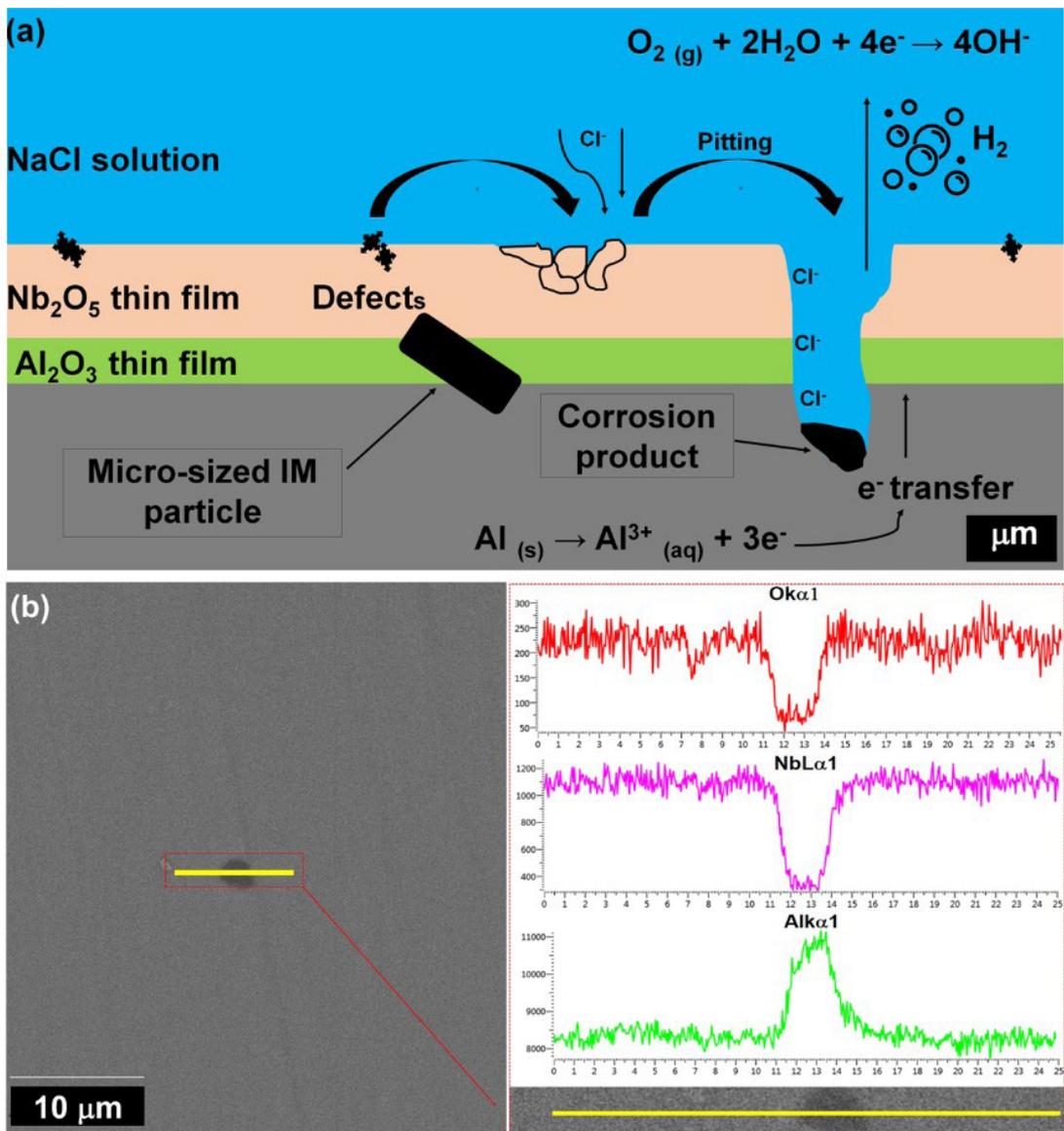
Figure 6. (a) schematic drawing to elucidate the corrosion mechanisms of coated 2198-T851 aluminium alloy exposed to an aggressive medium, and **(b)** SEM image, showing an uncovered region as well as the EDX spectra in the mentioned zone after 24 h of immersion in 0.6 mol L^{-1} NaCl solution.

As can be seen in Figure 7c a Pt block was deposited over the analysis region. The depth of the formed pit (see Figure 7d) on the 2198-T851 aluminium alloy surface is approximately 2.36 mm. EDX analysis carried out inside the pit showed the presence of Al, Cu, O and Si elements (see Figures 7 (e, f)). The presence of Si element may be related to the sanding process since it was accomplished with SiC sandpapers. The same procedure was applied for the 2198-T851 aluminium alloy containing Nb_2O_5 thin films. As can be seen in Figure 8 (a), the coated alloy has some defects on its surface, which are inherent to the reactive sputtering technique as mentioned before.

The region chosen for the cross-section is shown in Figure 8b, whilst the Pt block deposited on the region to be analysed can be verified in Figure 8c. Two cross-sections were performed, showing two different contrasts with depths of approximately 528.8 nm and 1.54 mm corresponding to Nb_2O_5 and base material (see Figure 8d), respectively. Considering the highest depth value for the coated material and comparing it with the base material, it was possible to confirm the Nb_2O_5 coating acts as a physical barrier. Figure 8e exhibits the SEM image obtained in the centre of the pit, and Figure 8f the EDX spectrum as well as the presence of Al, Cu, O and Nb elements.
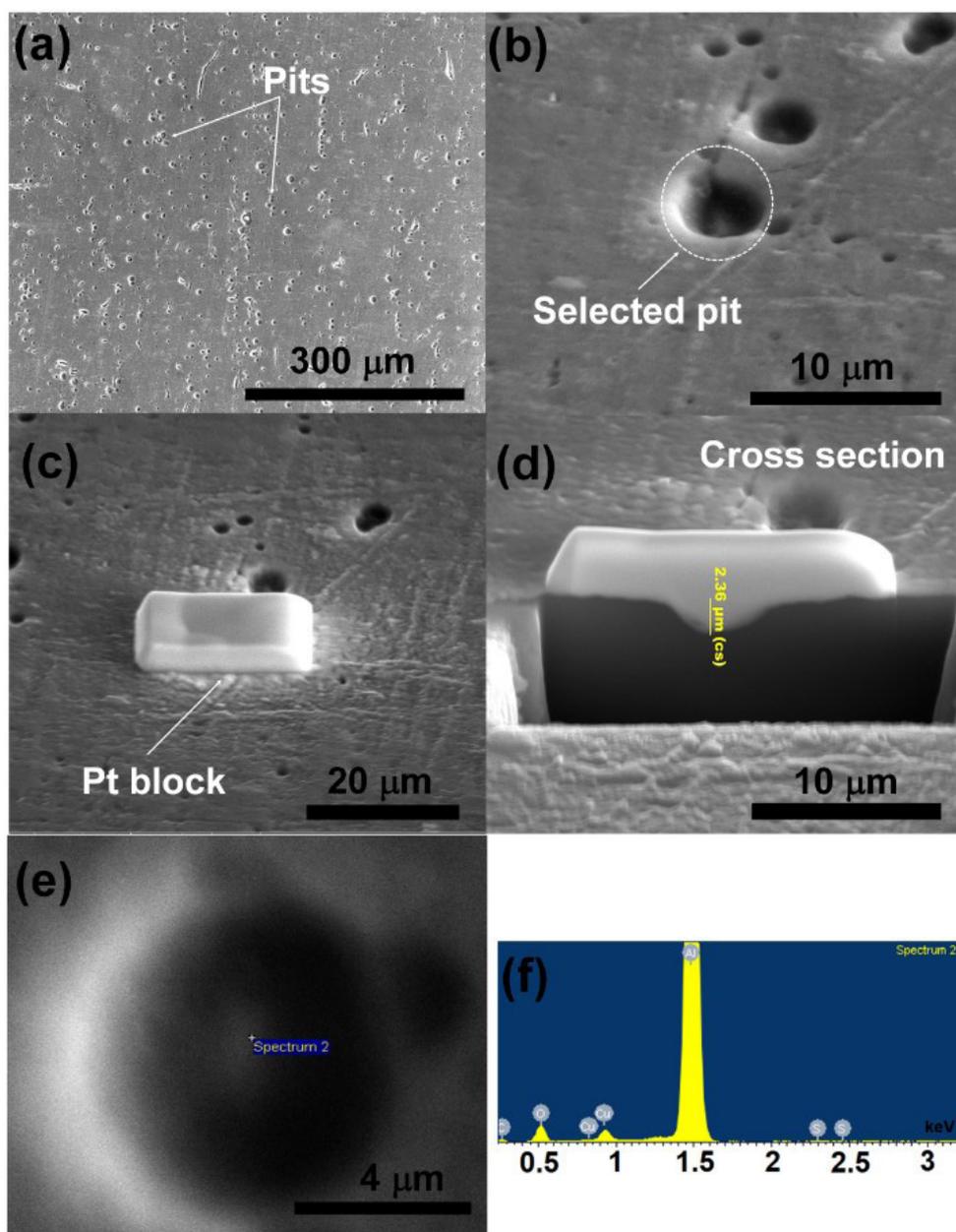
Figure 7. (a) An overview of the 2198-T851 aluminium alloy matrix as well as the pit distribution, **(b)** selected pit for the cross-sectional analysis, **(c)** presence of Pt block deposited on the pit region over the cross-sectional analysis, **(d)** cross-section image, demonstrating the pit depth, **(e)** SEM image in the centre of the pit, and **(f)** EDX spectrum displaying the presence of Al, Cu, O, C and Si elements.

As already mentioned in this manuscript, the nature of the corrosion products formed on the 2198-T851 aluminium alloy surface is still unknown. Thus, the combination of spectroscopic techniques such as Raman and XPS may help to shed some light on the corrosion mechanism of 2198-T851 aluminium alloy. While XPS provides surface elemental and chemical state composition of the top 10 nm (or thereabouts) or the surface of a material,

Raman spectroscopy provides molecular identification, including, in some cases, structural confirmation of a compound (corrosion products). Furthermore, the Raman technique allows the performance of specific analyses, which is extremely interesting for the present work. Finally, the two techniques are complementary and allowed the determination of corrosion products formed on the coated and uncoated 2198-T851 aluminium alloy.
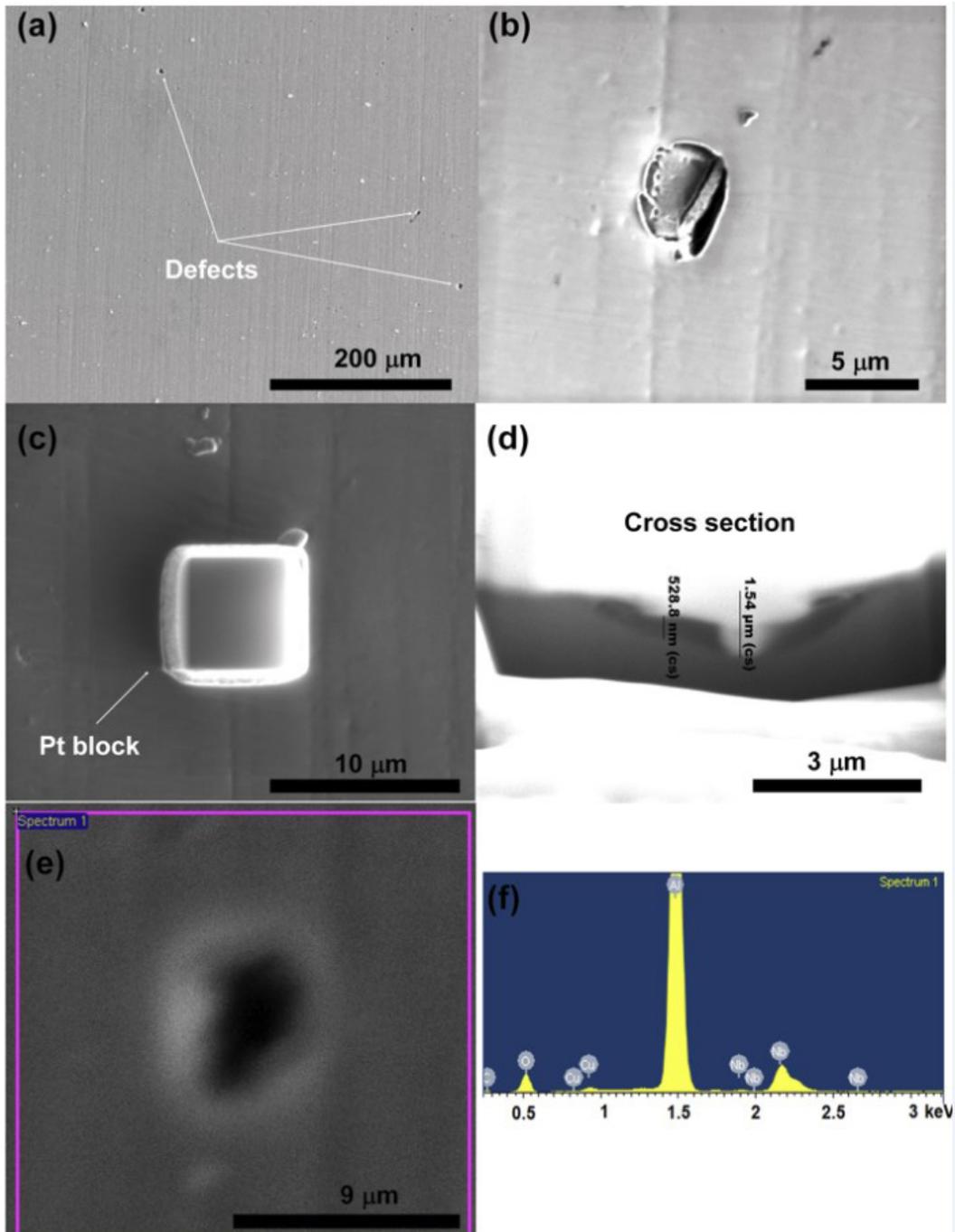
Figure 8. (a) An overview of the 2198-T851 aluminium alloy containing Nb_2O_5 thin film as well as the pit distribution, **(b)** selected pit for the cross-sectional analysis, **(c)** presence of Pt block deposited on the pit region over the cross-sectional analysis, **(d)** cross-section image, demonstrating the pit depths, **(e)** SEM image in the centre of the pit, and **(f)** EDX spectrum displaying the presence of Al, Cu, O, Nb and C elements.

For this purpose, different regions of the base material were analysed by using Raman spectroscopy, in search to understand the nature of corrosion products formed due to its exposure to 0.6 mol L^{-1} NaCl solution. Several Raman spectroscopy analyses (at different points and samples) for the specimens exposed to 24 h of immersion in 0.6 mol L^{-1} NaCl solution were performed. In fact, a small displacement of the bands can be verified for different samples. However, all values obtained were within the range expected and published in the literature. These findings show the reliability of the procedure adopted in the present work.

An overview of the 2198-T851 aluminium matrix after immersion testing is shown in Figure 9a. It is also possible to verify the regions chosen for the Raman spectroscopy analyses (Figure 9b). Figure 9c shows the intensity band in the range 250 - 300 cm^{-1}. The surface of 2198-T851 aluminium alloy containing Nb$_2$O$_5$ thin film after immersion testing (24 h of exposure) in 0.6 mol L^{-1} NaCl solution as well as detail of this uncovered region can be seen in Figure 10.
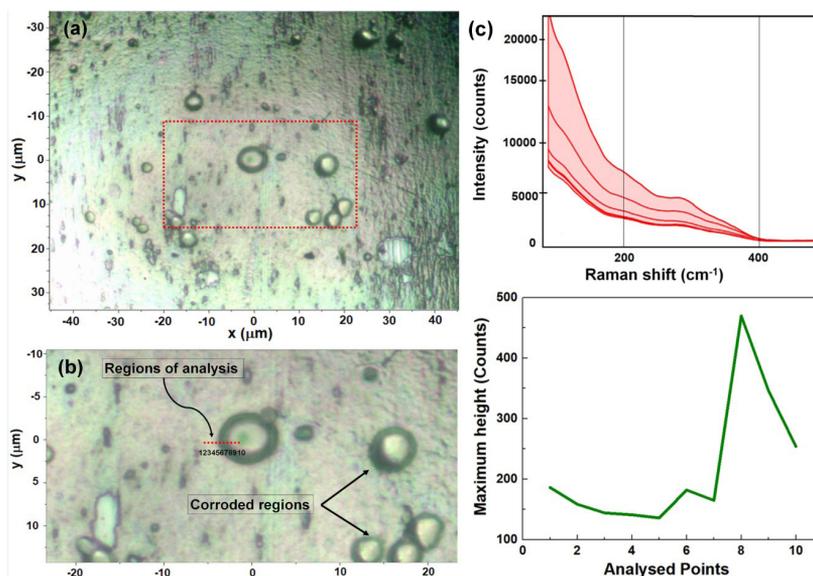
Figure 9. (a) An overview of the 2198-T851 aluminium alloy surface after 24 h of immersion in 0.6 mol L^{-1} NaCl solution, **(b)** selected points for Raman analysis, and **(c)** the intensity band in the range 250 to 300 cm^{-1}.
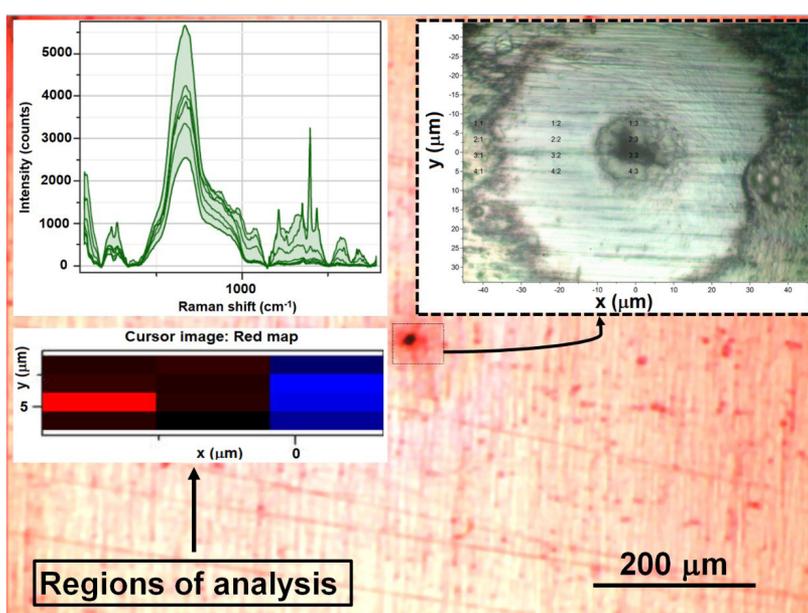
Figure 10. An overview of the 2198-T851 aluminium alloy coated with Nb$_2$O$_5$ thin film after 24 h of immersion in 0.6 mol L^{-1} NaCl solution and the detail of a pit formed on the sample surface. The inset on the right side shows the magnified region for Raman analysis as well as the selected points. The inset on the left side displays the Raman spectrum for these different regions of analysis.

Two regions of the spectrum were used to assemble the color intensity scale, proportional to the intensity of the band (Type: Height), where the red color shows the intensity band between 250 to 300 cm^{-1}, and the blue color shows the intensity band in the range 1385 to 1410 cm^{-1}.

Figure 11a presents the Raman spectra of the coated and uncoated 2198-T851 alloy after exposure to 0.6 mol L^{-1} NaCl solution. Spectra corresponding to the intervals used for the uncoated alloy analysis are displayed in Figures 11b and 11c, respectively. This result suggests dissolution of the 2198-T851 matrix and precipitation of amorphous aluminium hydroxide, $Al(OH)_3$, as revealed by the band centred at 234 cm^{-1}. The $Al(OH)_3$ precipitates at the top of the pit, forming amorphous domes and the hydrolysis reaction may be written as:

$$Al_{(s)} \rightarrow Al^{3+}_{(aq)} + 3e^- \tag{1}$$

$$Al^{3+}_{(aq)} + 3H_2O_{(l)} \rightarrow Al(OH)_{3(s)} + 3H^+_{(aq)} \tag{2}$$
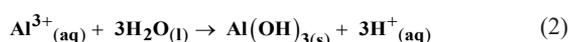
The strongest bands recorded in the range 405 to 215 cm^{-1} may be assigned to $CuCl_2 \cdot xH_2O$[24]. The band observed at 356 cm^{-1} is assigned by CuCl compound, and the bands centred at 501 and 586 cm^{-1} to the $Cu_2Cl(OH)_3$, respectively. Knowing the chemical composition of the 2198-T851 aluminium alloy as well as its corresponding Cu-rich particles, it is reasonable to infer the bands verified in the range 200 to 600 cm^{-1} may be directly associated to $Al(OH)_3$ and $Cu_2Cl(OH)_3$ as well as their intermediate compounds. Two bands were identified in the range 600 to 1000 cm^{-1} and, as mentioned in Drewien et al.[25], absorption bands for both stretching and deformation vibrations of aluminium oxide are present in this range. As reported by White and Hem[26], Raman spectra of the amorphous $Al(OH)_3$ gel exhibits a broad band ranging from 1060 to 1174 cm^{-1}, enabling numerous possibilities of association between oxygens of the carbonate ion as well as the aluminium in the gel. The band centered at 1085 cm^{-1} is related to the aluminium hydroxy carbonate[26] and the others (ranging from 1200 to 1440 cm^{-1}) to the vibrational modes of free carbonates[27]. As described in the literature[28],

the carbonates presence is governed by several environmental conditions, such as: CO_2 partial pressure, temperature, solution pH and atmospheric carbon. According to Zhang et al.[29], the hydroxycarbonates and hydroxychlorides present a similar structural, consisting of layered structures with the layers held together by anions ($CO3^{2-}$ and Cl^{-}) and is possible to verify the evolution from one phase to another through the ion-exchange mechanism as proposed by Odnevall and Leygraf[30] and more information can be found in reference. The analyses of intact areas showed a major band at 655 cm^{-1} as well as another around 206 cm^{-1} which may be attributed to Nb_2O_5[12,29,30].

Figure 12a shows a XPS survey spectrum for the uncoated 2198-T851 aluminium alloy revealing the presence of O, C, Al, Cu, and Cl. XPS results demonstrated the presence of $CuCl_2$ ($Cu3p_{3/2}$ 935.8, 78.8 and 80.0 eV) as well as CuCl or $Cu_2(OH)_3Cl$ (Cl2p / 200.7 eV; $Cu2p_{3/2}$ / 934.7 eV) as shown in Figure 12b. The fitting results of Al 2p are demonstrated in Figure 12c. As can be seen, two possible contributions were identified (Al_1 76.9 eV and Al_2 76.0 eV) which may be attributed to the AlO(OH), $Al(OH)_3$ and/or Al_2O_3 compounds. Since XPS measurements were performed using a non-monochromatic AlKα source the energy resolution is limited to untangling compounds that are too close to each other. Thus, for $Cl2p_{3/2}$ it is possible to observe only a single contribution around 200.7 eV which might be associated to CuCl and $Cu_2(OH)_3Cl$. A similar limitation occurs on Al2p. In this case, we have at least two compounds (Al_1 and Al_2) since a single component would not fit the peak. Interesting that according to literature the expected value for Al2p contribution of metallic aluminium and their alloys should appear around 73.0 eV. In this sense, the metallic contribution due to the passive film thickening and corrosion products cannot be observed. This limitation also happens for Cu2p signal that do not shows metallic contribution. These results corroborate with Bockris and Minevski[31], which attribute to the oxides a structure consisting of a base layer of Al_2O_3, in contact with the aluminium matrix, and in certain cases may present a surface area consisting mainly of $Al(OH)_3$.
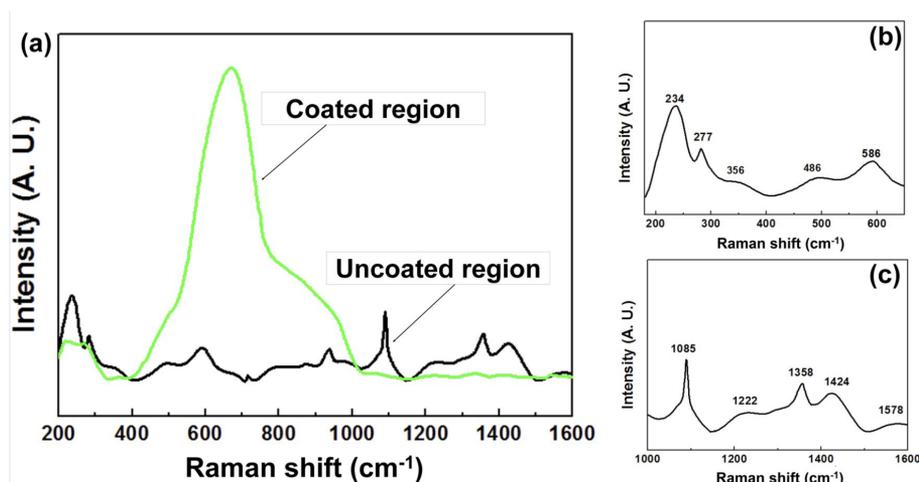
Figure 11. (a) Raman spectra of the coated and uncoated 2198-T851 alloy after exposure to 0.6 mol L^{-1} NaCl solution. **(b, c)** spectra corresponding to the intervals used for the uncoated alloy analysis.

The Al_2O_3 thin film is extremely effective to corrosion resistance[32] and present a thickness about 1 nm[33], while the average depth of the photoelectrons for Al2p is in the order of 10 nanolayers as reported by Briggs and Seah[34]. Figure 12d displays Cl_{2p} ($2p_{3/2}$ and $2p_{1/2}$) core-level spectrum for the uncoated 2198-T851 aluminium alloy, demonstrating the presence of CuCl compound. Figure 12e exhibits the XPS survey spectrum for the 2198-T851 aluminium alloy containing Nb_2O_5 thin film, whilst Figures 12fg show the fitting procedure of O1s and Nb 3d levels, respectively. Regarding the O1s spectra, it is important to note that due to the presence of several compounds at the surface,

it could not separate all possible contributions. In other words, it is reasonable to state that there are contributions of oxides as well as hydrocarbons and carbon oxides species at the surface for the sample as prepared. It was revealed the presence of a single niobium oxide phase (see Figure 12g), corresponding to Nb_2O_5 with binding energy for the Nb $3d_{5/2}$ of 208.9 eV and $3d_{3/2}$ of 211.6 eV, respectively[31,32]. Finally, the results obtained in the present work by using Raman spectroscopy associated to the XPS technique demonstrated to be a powerful tool for the assessment of the corrosion products of 2198-T851 aluminium alloy.
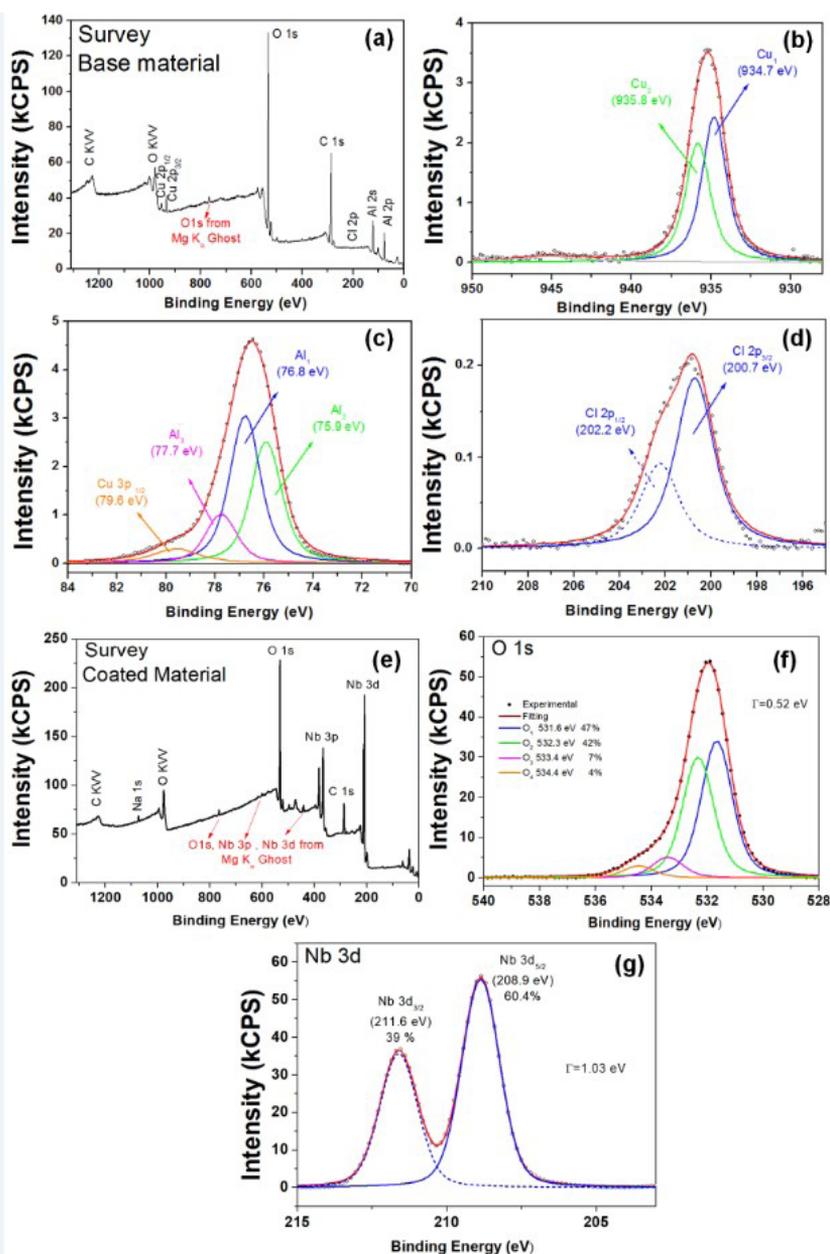
Figure 12. (a) XPS survey spectrum of 2198-T851 aluminium alloy, **(b)** Cu 2p, **(c)** Al 2p and Cu 3p, **(d)** Cl 2p, **(e)** XPS survey spectrum of coated 2198-T851 aluminium alloy, **(f)** O 1s levels, and **(g)** Nb 3d levels. All spectra were obtained for samples submitted to 24 h of immersion in 0.6 mol L^{-1} NaCl.

4. Conclusions

In the present work, the corrosion products formed on the 2198-T851 and 2198-T851/Nb_2O_5 aluminium alloy surfaces when exposed to sodium chloride solution were assessed by using Raman and XPS techniques. The immersion tests showed the Nb_2O_5 thin film deposited on the 2198-T851 aluminium alloy acts as a physical barrier layer against localised corrosion process. A severe localised corrosion process was verified for the base material, which presented a high pitting superficial density in the first hours of immersion as well as corrosion products. Remarkably, the 2198-T851 aluminium alloy containing Nb_2O_5 coating maintains its integrity during the first 15 h of immersion in 0.6 mol L^{-1} NaCl solution and the pit corrosion feature appears in 24 h of immersion. Raman spectroscopy revealed several corrosion products on the base material, such as $CuCl_2 xH_2O$ (405 to 215 cm^{-1}), CuCl (356 cm^{-1}), $Cu_2Cl(OH)_3$ (501 to 586 cm^{-1}) and $Al(OH)_3$ (234 cm^{-1}). XPS results for the uncoated material demonstrated the presence of $CuCl_2$ (Cu $3p_{3/2}$ 935.8, 78.8 and 80.0 eV) as well as CuCl or $Cu_2(OH)3Cl$ (Cl 2p / 200.7 eV; Cu $2p_{3/2}$ / 934.7 eV). Considering the fitting results of Al 2p, two possible contributions were identified (Al$_1$ 76.9 eV and Al$_2$ 76.0 eV) which may be attributed to the AlO(OH), $Al(OH)_3$ and/or Al_2O_3 compounds. The Cl_{2p} ($2p_{3/2}$ and $2p_{1/2}$) core-level spectrum exhibited the presence of CuCl compound. Considering the Raman analysis for the coated material, a major band at 655 cm^{-1} as well as another around 206 cm^{-1} may be attributed to Nb_2O_5. Corroborating with the Raman results, a single niobium oxide phase, corresponding to Nb_2O_5 with binding energy for the Nb $3d_{5/2}$ of 208.9 eV and $3d_{3/2}$ of 211.6 eV was determined by using XPS.

5. Acknowledgements

6. References

1. Sepe R, Giannella V, Razavi SMJ, Berto F. Characterization of static, fatigue and fracture behaviour of the aluminium-lithium alloy Al-Li 2198-T851. Int J Fatigue. 2023;166:107265. http://dx.doi.org/10.1016/j.ijfatigue.2022.107265.

2. Chen Y, Kong F, Yang J, Song X, Meng X. Damage behavior of 2198-T8 Al-Li alloy with different corrosion fatigue modes. Int J Fatigue. 2022;156:106671. http://dx.doi.org/10.1016/j.ijfatigue.2021.106671.

3. Decreus B, Deschamps A, Donnadieu P. Understanding the mechanical properties of 2198 Al-Li-Cu alloy in relation with the intra-granular and inter-granular precipitate microstructure. J Phys Conf Ser. 2010;240:012096. http://dx.doi.org/10.1088/1742-6596/240/1/012096.

4. Georgoulis D, Charalampidou CM, Alexopoulos ND. Corrosion resistance of aluminum alloy 2198 for different ageing tempers. Procedia Struct Integr. 2022;37:941-7. http://dx.doi.org/10.1016/j.prostr.2022.02.029.

5. Moreto JA, Marino CEB, Bose WW Fo, Rocha LA, Fernandes JCS. SVET, SKP and EIS study of the corrosion behaviour of high strength Al and Al–Li alloys used in aircraft fabrication. Corros Sci. 2014;84:30-41. http://dx.doi.org/10.1016/j.corsci.2014.03.001.

6. Donatus U, Terada M, Ospina CR, Queiroz FM, Bugarin A FS, Costa I. On the AA2198-T851 alloy microstructure and its correlation with localized corrosion behaviour. Corros Sci. 2018;131:300-9. http://dx.doi.org/10.1016/j.corsci.2017.12.001.

7. Araujo JVS, Donatus U, Queiroz FM, Terada M, Milagre MX, Alencar MC, et al. On the severe localized corrosion susceptibility of the AA2198-T851 alloy. Corros Sci. 2018;133:132-40. http://dx.doi.org/10.1016/J.CORSCI.2018.01.028.

8. Araujo JVS, Bugarin AFS, Donatus U, Machado CSC, Queiroz FM, Terada M, et al. Thermomechanical treatment and corrosion resistance correlation in the AA2198 Al–Cu–Li alloy. Corros Eng Sci Technol. 2019;54:575-86. http://dx.doi.org/10.1080/1478422X.2019.1637077.

9. Han J, Wang H, Xu A, Niu K. Enhanced matrix precipitation of T1 (Al$_2$CuLi) phase in AA2055 Al–Li alloy during stress aging process. Mater Sci Eng A. 2021;827:142057. http://dx.doi.org/10.1016/j.msea.2021.142057.

10. Ji Y, Xu Y, Zhang B, Behnamian Y, Xia D, Hu W. Review of micro-scale and atomic-scale corrosion mechanisms of second phases in aluminum alloys. Trans Nonferrous Met Soc China. 2021;31:3205-27. http://dx.doi.org/10.1016/S1003-6326(21)65727-8.

11. Lin Y, Li H, Wang Q, Gong Z, Tao J. Effect of plasma surface treatment of aluminum alloy sheet on the properties of Al/Gf/PP laminates. Appl Surf Sci. 2020;507:145062. http://dx.doi.org/10.1016/j.apsusc.2019.145062.

12. Moreto JA, Gelamo RV, Nascimento JPL, Taryba M, Fernandes JCS. Improving the corrosion protection of 2524-T3-Al alloy through reactive sputtering Nb_2O_5 coatings. Appl Surf Sci. 2021;556:149750. http://dx.doi.org/10.1016/J.APSUSC.2021.149750.

13. Freitas LR, Gelamo RV, Marino CEB, Nascimento JPL, Figueiredo JMA, Fernandes JCS, et al. Corrosion behaviour of reactive sputtering deposition niobium oxide based coating on the 2198-T851 aluminium alloy. Surf Coat Tech. 2022;434:128197. http://dx.doi.org/10.1016/j.surfcoat.2022.128197.

14. Ferreira MOA, Gelamo RV, Marino CEB, Silva BP, Aoki IV, Luz MS, et al. Effect of niobium oxide thin film on the long-term immersion corrosion of the 2198-T851 aluminium alloy. Materialia (Oxf). 2022;22:101407. http://dx.doi.org/10.1016/j.mtla.2022.101407.

15. Doniach S, Sunjic M. Many-electron singularity in X-ray photoemission and X-ray line spectra from metals. J Phys C Solid State Phys. 1970;3:285-91. http://dx.doi.org/10.1088/0022-3719/3/2/010.

16. Metikoš-Huković M, Babić R, Grubač Z, Brinć S. Impedance spectroscopic study of aluminium and Al-alloys in acid solution: inhibitory action of nitrogen containing compounds. J Appl Electrochem. 1994;24:772-8. http://dx.doi.org/10.1007/BF00578093.

17. Frankel GS. Pitting corrosion of metals: a review of the critical factors. J Electrochem Soc. 1998;145:2186-98. http://dx.doi.org/10.1149/1.1838615.

18. Tsutsumi Y, Nishikata A, Tsuru T. Pitting corrosion mechanism of Type 304 stainless steel under a droplet of chloride solutions. Corros Sci. 2007;49:1394-407. http://dx.doi.org/10.1016/j.corsci.2006.08.016.

19. Witharamage CS, Christudasjustus J, Smith J, Gao W, Gupta RK. Corrosion behavior of an in situ consolidated nanocrystalline Al-V alloy. Npj Mater Degrad. 2022;6:15. http://dx.doi.org/10.1038/s41529-022-00225-5.

20. Moreto JA, Broday EE, Rossino LS, Fernandes JCS, Bose WW Fo. Effect of localized corrosion on fatigue–crack growth in 2524-T3 and 2198-T851 aluminum alloys used as aircraft materials. J Mater Eng Perform. 2018;27:1917-26. http://dx.doi.org/10.1007/S11665-018-3244-7.

21. Araújo JVS, Silva RMP, Donatus U, Machado CSC, Costa I. Microstructural, electrochemical and localized corrosion characterization of the AA2198-T851 alloy. Mater Res. 2020;23. http://dx.doi.org/10.1590/1980-5373-mr-2020-0161.

22. Aliyu A, Srivastava C. Correlation between growth texture, crystallite size, lattice strain and corrosion behavior of copper-carbon nanotube composite coatings. Surf Coat Tech. 2021;405:126596. http://dx.doi.org/10.1016/j.surfcoat.2020.126596.

23. Ralston KD, Birbilis N. Effect of grain size on corrosion: a review. Corrosion. 2010;66(7):075005. http://dx.doi.org/10.5006/1.3462912.

24. Frost RL. Raman spectroscopy of selected copper minerals of significance in corrosion. Spectrochim Acta A Mol Biomol Spectrosc. 2003;59:1195-204. http://dx.doi.org/10.1016/S1386-1425(02)00315-3.

25. Drewien CA, Eatough MO, Tallant DR, Hills CR, Buchheit RG. Lithium-aluminum-carbonate-hydroxide hydrate coatings on aluminum alloys: Composition, structure, and processing bath chemistry. J Mater Res. 1996;11:1507-13. http://dx.doi.org/10.1557/JMR.1996.0188.

26. White JL, Hem SL. Role of carbonate in aluminum hydroxide gel established by raman and IR analyses. J Pharm Sci. 1975;64:468-9. http://dx.doi.org/10.1002/jps.2600640330.

27. Lopesino P, Alcántara J, de la Fuente D, Chico B, Jiménez J, Morcillo M. Corrosion of copper in unpolluted chloride-rich atmospheres. Metals (Basel). 2018;8:866. http://dx.doi.org/10.3390/met8110866.

28. Islam MM, Pojtanabuntoeng T, Gubner R, Kinsella B. Electrochemical investigation into the dynamic mechanism of CO_2 corrosion product film formation on the carbon steel under the water-condensation condition. Electrochim Acta. 2021;390:138880. http://dx.doi.org/10.1016/j.electacta.2021.138880.

29. Zhang X, Leygraf C, Odnevall Wallinder I. Atmospheric corrosion of Galfan coatings on steel in chloride-rich environments. Corros Sci. 2013;73:62-71. http://dx.doi.org/10.1016/j.corsci.2013.03.025.

30. Odnevall I, Leygraf C. Reaction sequences in atmospheric corrosion of zinc. ASTM Spec Tech Publ. 1995;1239:215-29.

31. Bockris JOM, Minevski LV. On the mechanism of the passivity of aluminum and aluminum alloys. J Electroanal Chem. 1993;349:375-414. http://dx.doi.org/10.1016/0022-0728(93)80186-L.

32. Ferreira SC, Rocha LA, Ariza E, Sequeira PD, Watanabe Y, Fernandes JCS. Corrosion behaviour of Al/Al_3Ti and Al/Al_3Zr functionally graded materials produced by centrifugal solid-particle method: influence of the intermetallics volume fraction. Corros Sci. 2011;53:2058-65. http://dx.doi.org/10.1016/J.CORSCI.2011.02.010.

33. Höpfner W. Handbook of Corrosion Data. 2nd Edition, hrsg. von Bruce D. Craig und David S. Anderson, ASM International Materials Park, OH 44073, Juni 1995, 998 S., $ 188,–, ISBN 0-87170-518-4. In Europa zu beziehen durch: American Technical Publishers Ltd., 27–29 Knowl Piece, Wilbury Way, Hitchin, Herts, SG4 OSX, England. Materials and Corrosion. 1996;47(1):53-4. http://dx.doi.org/10.1002/maco.19960470118.

34. Bubert H. Practical surface analysis A2, Vol. 1. Auger and X-ray photoelectron spectroscopy. 2. Auflage. Herausgegeben vonD. Briggs undM. P. Seah. Wiley, Chichester, Salle + Sauerländer, Aarau, 1994. 649 S., Broschur 49.95 £. – ISBN 0-471-9540-7. Angew Chem. 1995;107(11):1367. http://dx.doi.org/10.1002/ange.19951071133.